ADVANCED FUNCTIONAL MATERIALS
www.afm-journal.de

Mechanisms for High-Performance and Non-Local Photoisomerization Gratings in a Sol–Gel Material

Francisco Gallego-Gómez, Francisco del Monte, and Klaus Meerholz**

Novel azo-containing sol–gel films exhibiting outstanding properties for optical applications via nonlocal photoisomerization gratings were reported recently, although the underlying mechanisms were not well understood, especially regarding the unexpected non-local effect. Here, this photoisomerizable sol–gel material is characterized in-depth, analyzing the design and fabrication strategy, and discussing the aspects that enable the efficient photoresponse, with focus on the holographic recording. The material consists of an azochromophore-rich silica matrix containing glycidoxypropyl groups, which provide increased flexibility and internal free volume for improved dye photoresponse. The matrix characteristics allow a novel procedure for fabrication of thick optical films, in which chromophore aggregation is ruptured by thermal annealing while keeping the material centrosymmetry (beneficial for high hologram contrast). The molecular photo-orientation promotes alignment of microscopic domains in a cooperative motion, not reported previously in sol–gel materials. This collective mechanism enhances the material response and explains some intriguing features of photoisomerization gratings. In particular, there is evidence that spatially shifted domains are related to the grating nonlocal nature. Different recording (write–erase–write) procedures that distinctly affect the photoalignment at both molecular and microscopic level are studied. The holographic performance drastically changes, which can be selectively exploited for either long-term or dynamic holography.

1. Introduction

Holography provides a unique technique for high-density information storage and allows for a number of applications that are not accessible by other recording methods. Organic materials offer clear advantages not found in their inorganic counterparts because of their compositional and morphological versatility, easy processability, and low cost.[1] Photoanisotropic organic materials allow hologram recording without application of an electric field as a result of photoinduced anisotropy in the medium that, upon light absorption, becomes dichroic and birefringent (BR). Materials containing azobenzene-type chromophores (anisotropic, cigar-shaped molecules with the optical transition dipole moment lying along the long axis) constitute a representative example of BR systems achieved via photoisomerization (PI), based on *trans* → *cis* → *trans* transitions under exposure to polarized light:[2,3] successive PI cycles tend to line up the molecules in a dominant direction or plane, which ultimately provides macroscopic anisotropy. For a particular chromophore, the performance and stability of PI-induced alignment mainly depends on the chromophore interaction with the surrounding matrix.[4,5] Since 1984, PI systems have been proposed for holographic data storage[6] but their efficiency has been competitive in a few cases only[7,8] and generally inferior to, for example, organic photorefractive (PR) materials,[9,10] although the latter typically require high operating voltages.[11] Thus, there is a challenge in the design of new materials exhibiting highly efficient PI to become well-suited systems for holography. To achieve sufficient performance requires a good understanding of the mechanism governing the processes triggered by PI.

We have recently reported on the recording of PI gratings in a novel azo-containing sol–gel material exhibiting nearly total diffraction and subsecond response times.[12] Remarkably, a non-local nature of the PI gratings was assessed (i.e., they were out-of-phase relative to the interference light pattern), which had been assumed to be a unique feature of PR gratings. This allowed very high energy exchange between beams (optical gain) to be obtained, making PI materials suitable for applications based on signal amplification or phase conjugation. However, although the grating behavior was satisfactorily explained by a simple photoisomerization model, the material features and underlying mechanisms were not discussed. Here, we thoroughly characterize the material performance to elucidate the mechanisms responsible for the enhanced chromophore photoresponse and demonstrate cooperative motions at the microscale, which explain the unprecedented grating features. The article is structured as follows: first, we examine the strategy followed for material design regarding the composition

F. Gallego-Gómez,[+] K. Meerholz
Physical Chemistry Department
University of Cologne
Luxemburgerstrasse 116, 50939 Cologne, Germany
E-mail: francisco.gallegog@uam.es;
klaus.meerholz@uni-koeln.de
F. del Monte
Instituto de Ciencia de Materiales de Madrid (ICMM)
Consejo Superior de Investigaciones Científicas (CSIC)
C/Sor Angela de la Cruz 3, 28049 Madrid, Spain
[+] Present address: Departamento de Física de Materiales, Universidad Autónoma de Madrid, 28049 Madrid, Spain

DOI: 10.1002/adfm.201201281

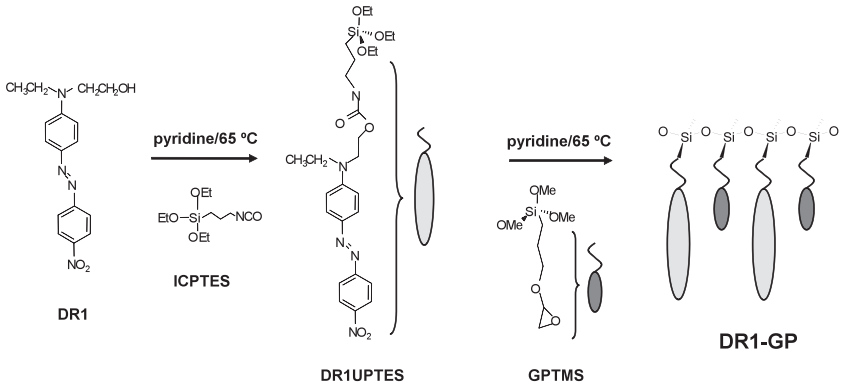

Scheme 1. Synthesis of **DR1-GP** by chemical functionalization of the alkoxyde precursor ICPTS and subsequent sol–gel process with GPTMS. Optically active (DR1-functionalized) groups are represented in light gray and optically non-active (GP) groups in dark gray.

and the fabrication process of thick optical films; second, we analyze the morphological features of the system, derived from film annealing, which allow material photoresponse; and, third, we investigate in-depth the holographic performance, particularly as affected by two-level (molecular and microdomain) photoalignment. In addition, our material is compared with a conventional azo-containing sol–gel system to underline the decisive factors improving the optical response.

2. Results and Discussion

2.1. Material Composition and Film Processing

The material of choice was organically modified silica, the composition and structure properties of which can be conveniently tailored.[13,14] To our purpose, silica was prepared via the sol–gel process combining two organic precursors; one optically active, the other one optically non-active (**Scheme 1**). The optically active precursor was prepared as described elsewhere;[15] briefly, the well-known azobenzene Disperse Red (DR1) was covalently bound to 3-isocyanatopropyltriethoxysilane (ICPTES) to obtain the DR1-functionalized alkoxyde precursor DR1UPTES. DR1 is a pseudo-stilbene-type (push–pull) molecule, characterized by strong overlapped π–π^* and n-π^* transition bands and a predominant *trans* state even under light exposure (metastable *cis* state),[2,16,17] so that light predominantly induces BR through molecular photoalignment (via angular redistribution).[16] The optically non-active precursor was glycidoxypropyltrimethoxysilane (GPTMS). Thereby, glycidoxypropyl (GP) groups pending from the silica network are intended to play the simultaneous roles of silica network plasticizer and spacer between adjacent DR1 molecules. Both aspects should improve chromophore reorientation upon PI by i) providing more internal free volume to favor dye motion,[18] ii) restricting chromophore-chromophore interactions and aggregation,[19,20] and iii) increasing the flexibility of the silica matrix (decreasing T_g).[2] The lower T_g should also facilitate network reorganization due to external stimuli (e.g., thermal treatment or illumination), which could even promote motion of microscale domains.[3]

The sol used for hydrolysis and condensation was composed of 1 mmol of each precursor so that the final composition was DR1UPSiO$_{1.5}$(1)–GPSiO$_{1.5}$(1) in molar equivalents (75:25 w/w). The resulting sol–gel material is hereafter referred to as **DR1-GP**. The corresponding amount of DR1 was 52 wt%, which was confirmed by thermogravimetric analysis. The strong covalent attachment of the dye to the silica backbone allowed such a high load of DR1 without phase segregation and crystallization problems.[15] Otherwise, direct incorporation of DR1 (i.e., without previous synthesis of DR1UPTES) led to unstable materials above 20 wt% compositions. In order to evaluate the eventual benefits of the incorporation of optically non-active groups, we prepared a second set of samples using tetraethyl orthosilicate (TEOS, typically used in azo-containing sol–gel materials)[15,21] instead of GPTMS. This reference material, referred to as **DR1-TEOS**, had a final composition of DR1UPSiO$_{1.5}$(1):SiO$_2$(1) in molar equivalents (88:12 w/w).

Reproducible plane-parallel, thick (2 to 102 μm) films, having large area and high optical quality, could be easily fabricated following the procedure described in the Experimental Section. If the **DR1-GP** material is allowed to gelation without further processing, the resulting films exhibited massive DR1 aggregation as revealed by the presence of a shoulder at approximately 420 nm[19] in the absorption spectrum (**Figure 1**). It is well known that hydrolysis and condensation of silane precursors occur around aggregates[22] so that they persist after

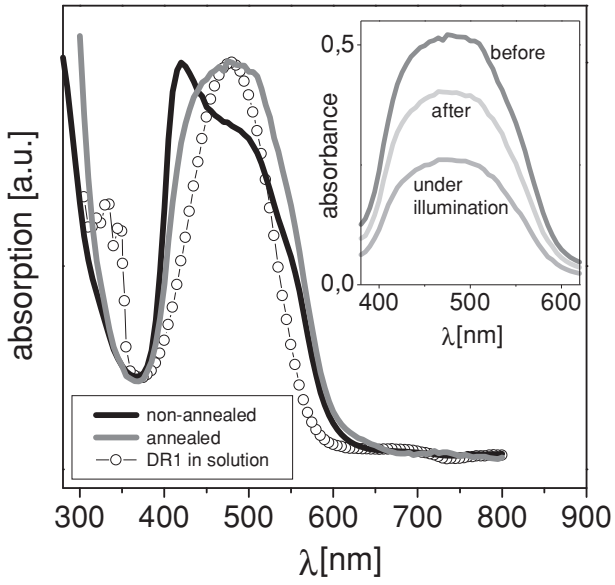

Figure 1. UV-Vis spectra of 2 μm thick **DR1-GP** films, either subjected or not to thermal annealing. Chromophore dimeric aggregation, evidenced by the peak at 420 nm, is ruptured by the thermal treatment. For comparison, the spectrum of DR1 in solution is also shown, exhibiting the characteristic absorption of non-aggregated DR1 species centered at 480 nm. Inset: spectral changes in the annealed **DR1-GP** film during and 90 min after illumination with linearly polarized 633 nm light (200 mW cm^{-2}, normal incidence). The absorbance, in all cases, was basically independent of the polarization of the probe light (spectrometer lamp). No absorbance change was observed in non-annealed **DR1-GP** films.

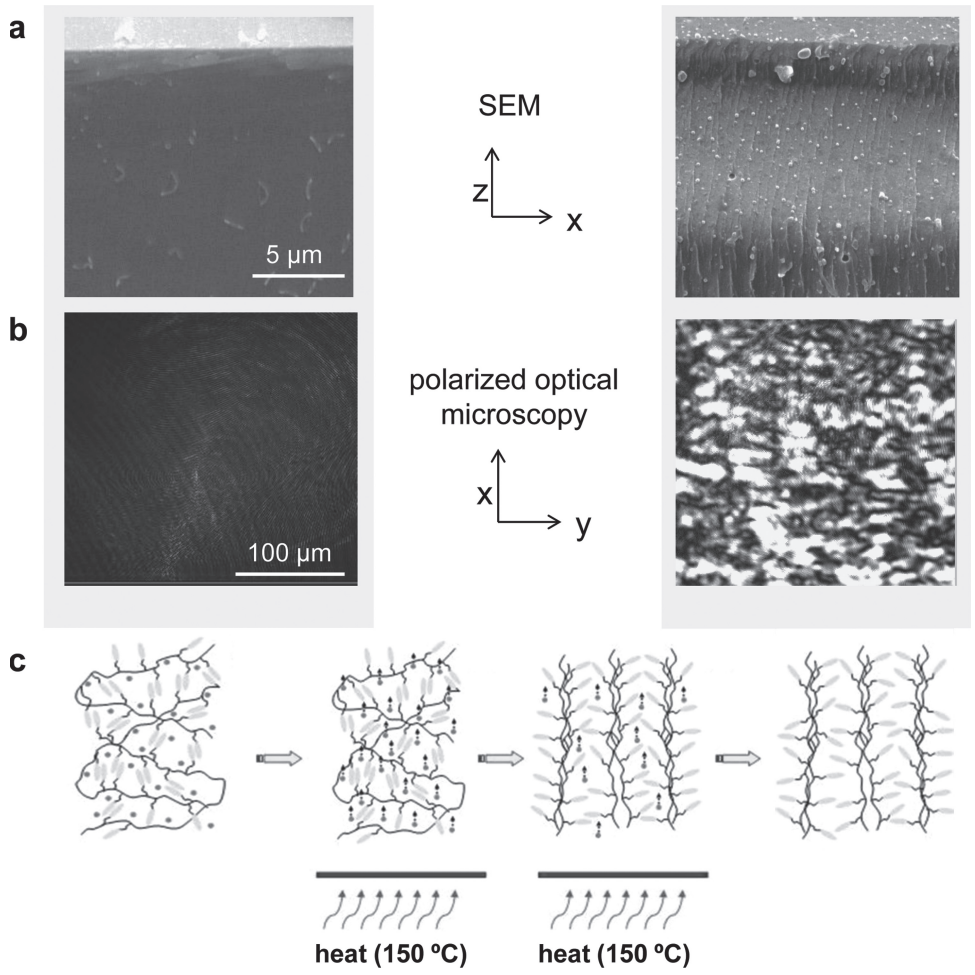

Figure 2. a) Cross-sectional SEM images and b) POM images of non-annealed (left) and annealed (right) 12 μm **DR1-GP** films. Microscope light polarization in POM was 45° with respect to the *x*-axis. c) Idealized matrix reorganization occurring upon annealing and solvent evaporation. Black lines represent the silica network; blue rods, the DR1-functionalized groups; and circles, entrapped molecules of pyridine. Circular fringes in (b) are an optical artifact. The *z*-axis represents a direction normal to the sample while (*x*, *y*) are in the film plane.

gelation. Aggregation is typically undesirable because of the detrimental effect on PI processes.[3,19] This was actually the case in our films, the response of which to illumination was negligible, except for the photoinscription of surface relief gratings (SRGs) by an interference pattern, as we observed by atomic force microscopy (AFM). However, the SRGs were slightly pronounced, with depth less than 400 nm. The film did not respond to external poling either (even by applying electric fields as high as 100 V μm^{-1}).

Thus, aggregation rupture was mandatory to obtain any optical response. This was achieved by subjecting the material before complete gelation to abrupt heating by placing the sample on a hot plate at 150 °C (see the Experimental Section). Indeed, effective elimination of dye aggregates was verified by the disappearance of the 420 nm shoulder in the absorption spectrum (Figure 1). As an immediate consequence, the annealed film became responsive to optical stimulus as DR1 molecules were now capable of PI-induced alignment. This was readily confirmed by measuring in situ the film absorbance (*A*) during and after illumination (Figure 1, inset). Under linearly polarized 633 nm irradiation[23] (normal incidence), the absorbance significantly reduced independently of the probe light polarization, i.e., both perpendicular ($A_\perp$) and parallel ($A_\parallel$) absorbances were identical to that measured with unpolarized probe light (A_0). This indicates that DR1 molecules became preferentially photoaligned along the propagating direction of the pump light (out-of-plane alignment).[24] Similar behavior, different to conventional PI, has been observed in other photoisomerizable systems, particularly under illumination at 633 nm.[5,25,26] After irradiation, DR1 molecules relaxed back to random orientation and *A* was partially recovered. The spectral shape did not change during the experiment.

3. Film Morphology Enabling Optical Response

3.1. Matrix Rearrangement Upon Film Annealing

The drastic effect of film annealing revealed that important morphological changes were induced in the material. Further evidence of such changes was provided by scanning electron microscopy (SEM). **Figure 2**a shows a homogeneous bulk in

non-annealed **DR1-GP** films after non-interfered gelation while annealed films presented a striped bulk, with approximately 1 μm thick bands disposed normally to the substrate, which points to a microscopic matrix arrangement. This organization was also observable with polarized optical microscopy (POM), which, in addition, revealed some degree of anisotropy in the rearranged matrix[27] (Figure 2b). Indeed, non-annealed films appeared as a plain dark field corresponding to a homogeneous, isotropic bulk. On the contrary, bright areas appeared in the annealed samples, indicating anisotropic domains of tens of microns. This suggests microphase separation with formation of silica-rich domains (essentially isotropic) and DR1-rich domains (anisotropic), the latter showing birefringence as a result of some preferred direction for chromophore arrangement. POM images barely depended on the polarization of the incoming probe light, suggesting that the anisotropy of the annealed film has uniaxial symmetry (normal to the sample surface), in accordance to the vertical structures observed in SEM.

All these observations compose a scenario consistent with an evaporation induced self-assembly (EISA) process[28] upon film annealing (Figure 2c). The sudden increase of temperature before complete gelation promoted both the softening of the GP-modified silica network (with T_g about 100 °C)[12] and the prompt evaporation of remaining pyridine (boiling point is 90 °C). Under these circumstances, solvent evaporation and diffusion through the bulk (from the bottom of the sample to the top) caused drifting and reorganization of the softened silica matrix, and simultaneous rupture of dye aggregates. Thus, the vertical structures observed in SEM images can be attributed to well-ordered silica chains. Such bulk structuring in samples of thickness over several microns is remarkable since efficient EISA-like assembly is typically restricted to several tens of nanometers.[28] The persistence after cooling of the morphological changes indicates that the silica backbone retained the arrangement, probably favored by an increase of rigidity in the quenched network. This was confirmed by stiffness measurements with nanoindentation, yielding a clear increase of the Young's modulus in annealed films (ca. 32 GPa) with respect to non-annealed samples (ca. 20 GPa). Such mechanical hardening, together with the presence of GP groups acting as spacers between DR1 molecules, prevented the formation of new dye aggregates after annealing. Permanent chromophore disaggregation upon annealing has also been observed in other highly amorphous azo-containing systems (polymers[19] and sol–gel materials).[29]

3.2. Optical Properties: Centrosymmetry and Photoinduced Birefringence

As the EISA-like reorganization also involves the organic moieties, annealing can lead (before photoexcitation) to material birefringence if the chromophore adopts an anisotropic distribution in the annealed **DR1-GP** films, or even to material non-centrosymmetry if the dipolar DR1 molecules point towards a preferred direction.[30] On the one hand, fairly low electro-optic (EO) coefficients (r_{13} = 0.3 pm V^{-1} and r_{33} = 1.2 pm V^{-1}) were measured,[12] indicating that the orientation of dye dipoles was approximately random (with slight alignment in the *z*-direction) after annealing and the material was nearly centrosymmetric. Further, the negative sign of r_{33} reveals a certain tendency of the chemically bound chromophores to point their unbound nitro group towards the film–air interface rather than the film–glass interface, which is a consequence of the EISA process. On the other hand, ellipsometry demonstrated that, right after annealing, **DR1-GP** films exhibited low but non-vanishing birefringence ($|n_e - n_o| \approx 0.03$), which agrees with the fact that r_{33} was higher than r_{13}. This initial BR is also consistent with the recognizable structures in POM images, which already revealed some film anisotropy. Both EO and ellipsometric measurements were basically insensitive to electrical poling of the films, even at fields as high as 100 V μm^{-1}. This demonstrated that the high-T_g matrix (even with the incorporation of GP groups) hindered the capability of the DR1 molecules to reorient along an electric field.

The main effect of annealing was to provide the material with a photoresponse, as readily demonstrated by the absorbance changes under illumination in annealed films (Figure 1, inset). This is attributed to the matrix reorganization achieved during annealing, which enabled DR1 molecules to exhibit PI-induced alignment. Such optical response, allowing the photoinduction of BR, was even observable by POM, demonstrating long-range matrix reordering upon illumination (**Figure 3**a, showing a 2 μm thick sample).[31] Indeed, isotropic–anisotropic microstructures underwent rearrangement under 633 nm irradiation towards higher birefringence (brighter stripes at t_1 compared to t_0, for better comparison, only the left half of the sample was exposed to light). Changes occurred over several microns, revealing that chromophore alignment due to PI took place not only at the molecular level, but also in microscopic domains due to cooperative motions. This was probably favored by the high concentration of PI chromophores covalently bonded to an organized structure. This also demonstrates that, even after annealing, the silica network was flexible enough, in spite of its high-T_g, to allow conformational rearrangement on microscopic scale, although restricting back relaxation, so the effect was only partially reversible. Thus, after blocking the light, the structures slowly tended to a somewhat different state (t_2) compared to the original one (t_0). By contrast, the right half of the sample, several tens of microns apart from the irradiated area, remained unchanged. Microscale photomechanical motions have previously been described in azo-containing liquid-crystalline and photoaddressable polymers[3,8,24,32] and in some small molecules,[33] leading to overall enhancement of the optical response. Nevertheless, their occurrence has not been demonstrated in high-T_g sol–gel materials previously.

Ellipsometry was employed to monitor the PI-induced material anisotropy of **DR1-GP** films (Figure 3b). Irradiation by 633 nm light (200 mW cm^{-2}) induced a strong increase of BR (transmitted signal I_{ELP} increased), which reached remarkable values ($|n_e - n_o|$ = 0.09 and 0.11 in 12 μm thick films exposed to light for 300 and 5000 s, respectively), close to the best values ever reported for photoinduced anisotropy in hybrid materials.[25,34] After switching the light off, the BR decreased only partially and retained around 60% of the maximum value achieved, in accordance with the permanent spectral change showed in Figure 1, inset. The slow and incomplete back relaxation (over

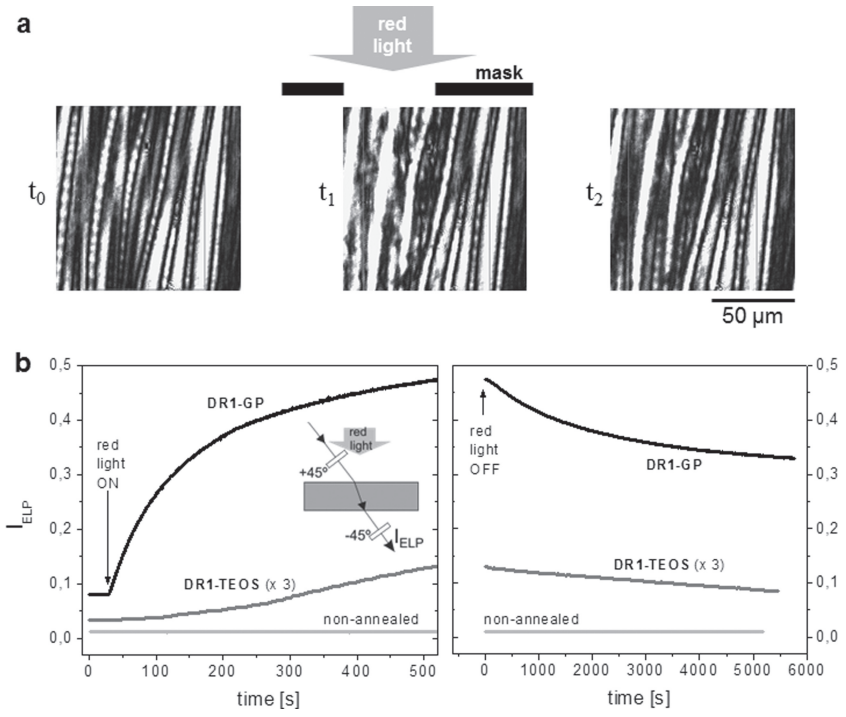

Figure 3. a) Evolution of an annealed 2 µm thick **DR1-GP** film under uniform irradiation observed by POM: prior to illumination (t_0), after illumination for 3 min (t_1) and after relaxation for 45 min in the dark (t_2). For better comparison, only the left half of the sample was exposed to light. b) Ellipsometric transmission of 12 µm thick samples during uniform illumination (left) and subsequent relaxation in the dark (right –note the longer time scale). **DR1-GP** (annealed and non-annealed) and **DR1-TEOS** (three-fold magnified) films are compared. In all cases, samples were irradiated with a polarized 633 nm laser (200 mW cm^{-2}) with normal incidence (see inset).

more than 90 min) reflects the difficulty of the azo-molecules to spontaneously randomize in a viscous environment, in which, additionally, the chromophore mobility is restricted by the strong covalent bond to the high-T_g matrix.[35] Nevertheless, the degree of (spontaneous) reversibility is higher than that typically found in azo-based systems,[3,8,34,35] likely due to the GP-containing silica network. The decay of I_{ELP} fits a biexponential function with typical fast and slow constant times of 5–10 s and 200–400 s, respectively, which is compatible to the distinct molecular and domain relaxation times. EO coefficients barely changed upon 633 nm illumination (by less than 0.3 pm V^{-1} at exposure of 200 mW cm^{-2} for 15 min), which indicates that PI provoked chromophore alignment (BR strongly increased) rather than dipole orientation (the film remained centrosymmetric). Light exposure induced no observable changes in SEM images, supporting that the vertical structures correspond to silica arrangements.

For comparison, **DR1-TEOS** samples were also analyzed. In this material, film annealing at 150 °C barely had influence on the optical properties, likely due to the higher matrix T_g (ca. 145 °C); note that annealing at higher temperature led to progressive thermal degradation of DR1. No anisotropic domains were observed by POM. Figure 3b also demonstrates significantly poorer dye photoalignment than **DR1-GP**, exhibiting PI-induced BR about one order of magnitude smaller and 20-fold slower (note that both **DR1-TEOS** and **DR1-GP** films showed identical absorption at 633 nm). This demonstrates the strongly beneficial incorporation of GP groups to the silica network, as intended. On the other hand, the more rigid matrix of **DR1-TEOS** probably allowed optical response in non-annealed films by preventing strong dye aggregation. By contrast, non-annealed **DR1-GP** films showed no response to illumination (Figure 3b) or electrical poling. They exhibited perfect isotropy at any time, i.e. negligible BR ($|n_e - n_o| < 10^{-4}$) and vanishing EO coefficients ($|r_{11}|, |r_{33}| < 0.02$ pm V^{-1}).

4. Holographic Performance

The large PI-induced birefringence observed in **DR1-GP** makes this material suitable for holographic recording without applying electric field. Indeed, high-performance holograms were obtained by interfering two 633 nm write beams (WBs) in the film to induce modulated photoalignment of the DR1 molecules, that is, the PI grating (see the Experimental Section). Near 100% diffraction efficiency (h), large refractive index change (Δn, beyond 10^{-2}) and very high optical gain (gain coefficient Γ up to 900 cm^{-1}) were achieved.[12] The latter fact further revealed that PI gratings can exhibit spatial shift with respect to the interference light pattern.[1] A contribution of photorefractivity was ruled out because of, among other reasons, the absence of photogeneration agents in the material, leading to vanishing photoconductivity in the films.[12] Further, no SRGs were now photoinscribed in annealed **DR1-GP** films (as verified by AFM), probably due to the increased matrix rigidity after thermal treatment.

Here we analyze the holographic performance with emphasis on those aspects revealing the mechanisms responsible for the material behavior. First, we underline the key material properties that enable the improved holographic response. Second, we discuss the occurrence of PI-induced cooperative motions explaining some intriguing grating features. And third, we investigate the recording reversibility/stability under different grating erasure procedures, which provides further fundamental insights into the photoprocesses involved.

4.1. Improving Material Properties

i) As outlined above, GP groups provided both flexibility and free volume to the silica network and diminished chromophore-chromophore interactions in the annealed matrix. Similarly to BR response, these factors led to a much superior holographic performance of **DR1-GP** compared to **DR1-TEOS** (**Table 1**), not only in terms of h and Γ, but also regarding the buildup times (τ_{50}). In both materials, the grating response times were similar to those of PI-induced birefringence (ellipsometry), confirming the obvious correlation between both phenomena.

Table 1. Steady-state grating properties (η and Γ) and corresponding buildup half-times (τ_{50}) of gratings recorded in different materials. Recording transmission geometry ($\theta_1 = 26°$, $\theta_2 = 34°$) was used. Sample thicknesses were 12 μm.

	η [%]	τ_{50} (η) [s]	Γ [cm^{-1}]	τ_{50} (Γ) [s]
DR1-GP	52	43	(670	62
DR1-GP (prepoled)	20	49	(290	65
DR1-GP (non-annealed)	0	–	0	–
DR1-TEOS	6	850	(40	1040
DR1-TEOS (non-annealed)	4	900	(25	1120

ii) The material preparation preserved the symmetry of the films, as discussed above. Thus, by holographic recording, the azo-molecules became aligned in the bright fringes and remained randomly oriented in the dark ones, leading to high grating contrast. By contrast, most azo-containing materials previously reported for holography were poled, optically or electrically, prior to or during grating recording. According to this, dye molecules were also aligned in the dark fringes, leading to diminished grating performance. To confirm this, films were subjected to corona poling during the annealing, which was identical to that in the standard films. After cooling, permanent field-induced alignment of the polar DR1 molecules was verified by ellipsometry ($|n_e - n_o| \approx 2 \times 10^{-3}$ without illumination, slightly superior to values reported in similar systems,[15] probably due to presence of GP groups). Holograms recorded in these pre-poled films were significantly weaker (lower η and Γ), although showing similar response times (Table 1). The latter fact suggests that the chromophore motion in the pre-poled sample was barely altered by the poling, so the poorer performance was, in fact, due to worse grating contrast rather than hindered chromophore orientability. A similar detrimental effect occurred if the sample was uniformly illuminated prior to grating recording (which is a procedure used in PR polymers to increase the speed).[36] Therefore, gratings were standardly recorded by promptly opening both WB's.

iii) The matrix arrangement (including efficient rupture of dye aggregation) achieved by the EISA process during annealing (Figure 2) appears as a paramount aspect to obtain optical response. In fact, no holograms could be written in non-annealed **DR1-GP** films (Table 1). The incorporation of GP groups lowered the matrix T_g, enabling efficient annealing at 150 °C, i.e., below dye degradation temperature. By contrast, as previously mentioned, the higher matrix T_g of **DR1-TEOS** likely allowed some holographic performance without annealing (Table 1) but strongly reduced the improving effect of thermal treatment. The relevance of the matrix ordering in our material was further corroborated as the performance worsened in thicker samples. **Figure 4** shows a drastic decrease of Δn and Γ (both thickness-independent parameters)[1] and a clear slowdown of the buildup by increasing film thickness. This indicates more efficient matrix reorganization by annealing in thinner samples, therefore better suited for holographic recording. It must be noted that, given the high absorption of our material, light penetration significantly reduced in thick samples, which

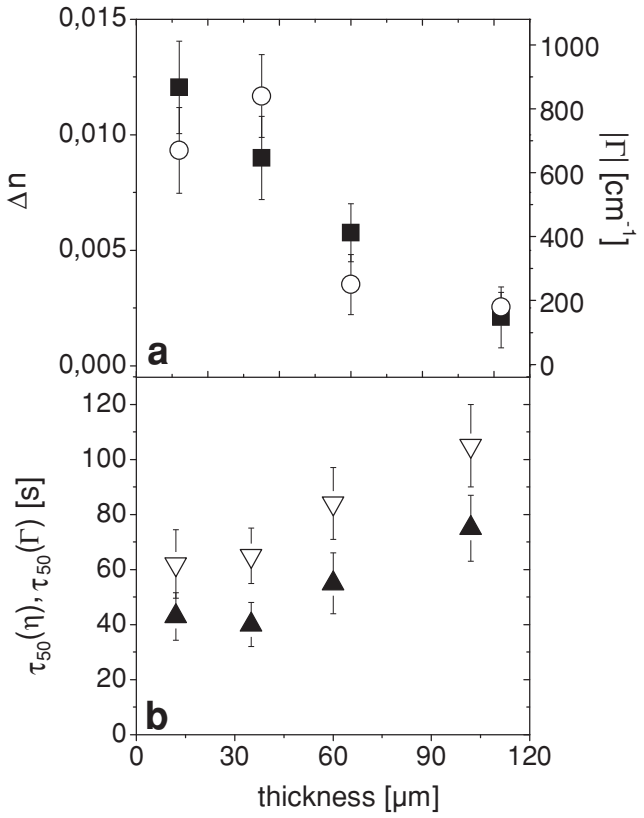

Figure 4. Thickness-dependence of: a) the steady-state grating properties (Δn and $|\Gamma|$, solid and open symbols,respectively) and b) the corresponding buildup times ($\tau_{50}(\eta)$ and $\tau_{50}(\Gamma)$, solid and open symbols, respectively) of holograms recorded in **DR1-GP** films with varying thicknesses. A recording transmission geometry ($\theta_1 = 26°$, $\theta_2 = 34°$) was used. Data and error bars are, respectively, average values and their standard deviations of measurements performed on 5 different samples of each thickness.

surely reinforced the observed trend. However, as the grating dynamics for a given sample thickness is basically independent of the recording light intensity,[12] the slower response times in thicker samples confirm that the tendency is mainly related to worsening of the matrix reorganization. This agrees with typical behavior when solvent gradients are used for structural organization of films:[28] the thinner the film, the better the order of the resulting structures.[37] In any case, annealing induced significant volume ordering even in samples as thick as 100 μm.

4.2. Cooperative Motions: Two-Level Mechanism

The POM images in Figure 3a revealed film rearrangements over several microns upon illumination, which strongly suggested that chromophore photoalignment triggered motions along microscopic domains as a result of collective processes in our material. We verified the existence of such a cooperative effect in our material by alternatively interrupting and resuming the hologram recording (**Figure 5**). After partially recording the grating, both WBs were briefly blocked. Over this period, the

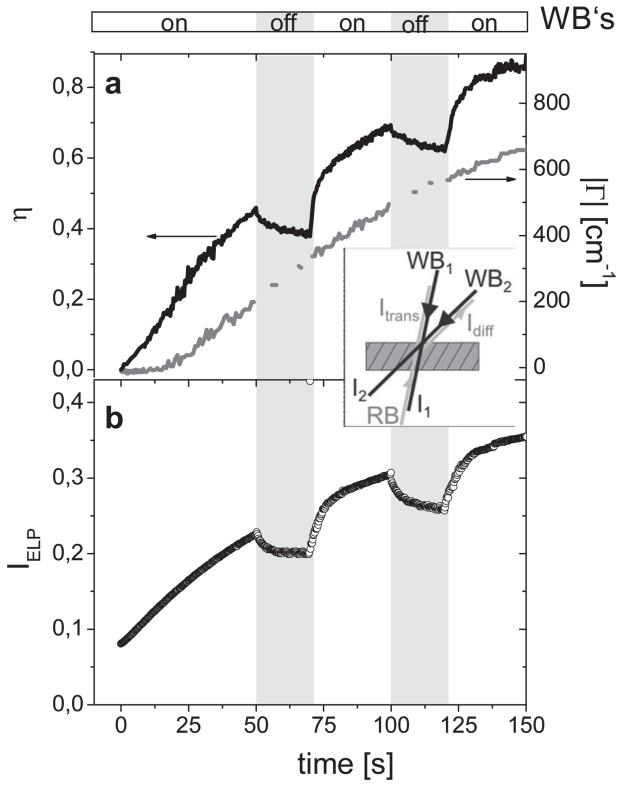

Figure 5. Temporal evolution of: a) the grating properties η and Γ, and b) the simultaneous ellipsometric transmission measured in a 35 µm **DR1-GP** film. Both write beams were blocked between t = 50 and 70 s and between t = 100 and 120 s (in these intervals, the WBs were briefly opened to measure Γ). A recording transmission geometry (θ_1 = 26°, θ_2 = 34°) was used. Inset: scheme of the grating recording and read-out (see the Experimental Section).

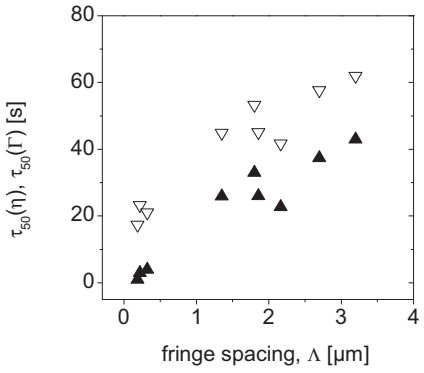

Figure 6. Grating buildup half-times ($\tau_{50}(\eta)$ and $\tau_{50}(\Gamma)$, solid and open symbols, respectively) as function of the fringe spacing Λ. Holograms were recorded in 12 µm **DR1-GP** films using different recording transmission and reflection geometries.

aligned azomolecules within the bright fringes randomly reoriented via thermal relaxation. Consequently, both the induced birefringence and the grating contrast diminished (I_{ELP} and η decreased). By resuming the recording (WBs were unblocked), both I_{ELP} and η rapidly recovered the values corresponding to an uninterrupted recording. Most revealing, Γ continued its trend fully undisturbed, i.e., the grating shifted further from the interference pattern during the dark period (the η decrease was small enough not to affect Γ).

This behavior strongly conveys the occurrence of two orientational mechanisms, each having its individual kinetics: the first one based on chromophore alignment upon PI in a relatively short time-scale (a few seconds or less); the second one based on cooperative motion of microdomains, driven by the aligned chromophores covalently bound to the matrix, which occurs over longer times (tens of seconds) since it involves rearrangement of the silica network rather than simple conformational changes. Upon interrupting the illumination for a short period, chromophore alignment is partially randomized within the domains (so I_{ELP} and η decrease) while the domains keep their emplacement within the film. They continue to pull off the silica network, the drift of which leads to further shift of the grating from the light pattern, so Γ increases even in the dark. Thus, the molecular alignment appears to mainly govern the grating modulation (diffraction efficiency) while the domain motion rather affects the grating shift (optical gain). By resuming the recording, dye molecules need to reorient again but not the domains, so the grating is rapidly recovered. These features are further discussed in the next section.

Two further observations corroborate the proposed scenario. On the one hand, the role of microdomains in the grating shift agrees with the delayed occurrence of optical gain with respect to diffraction. This is evident in the initial stage in Figure 5 as well as in the buildup half-times, $\tau_{50}(\Gamma)$ being always higher than $\tau_{50}(\eta)$ (Table 1, Figure 4, and **Figure 6**). On the other hand, there is a direct correlation between the dimensions of the interference fringes and the grating dynamics (Figure 6). By recording with transmission geometries, the interference pattern has broad fringes of some microns, so the PI grating buildup involves realignment of whole microdomains. Indeed, buildup response times of transmission gratings range tens of seconds, which corresponds to the time scale of microscopic conformational changes. By contrast, reflection gratings have much narrower fringes (ca. 0.2–0.4 µm), so the grating formation requires alignment of chromophore rather than of domains. Accordingly, much faster buildup times (with $\tau_{50}(\eta)$ of a few seconds and even sub-second) were measured. Nevertheless, $\tau_{50}(\Gamma)$ values were still in the range of tens of seconds, which agrees with the relevance of domain motion in the attaining of optical gain, as proposed above. Note that the steady-state values of η and Γ did not depend directly on the fringe spacing but rather on the Poynting vector in each recording geometry, as found in the literature.[12]

4.3. Reversibility of the Holographic Recording: Grating Mechanisms

Grating stability and reversibility are crucial properties for material applicability. While long grating lifetimes after recording are mandatory for long–term information storage, erasability and rewritability are indispensable for dynamic applications. Several recording schemes were examined to address these issues,

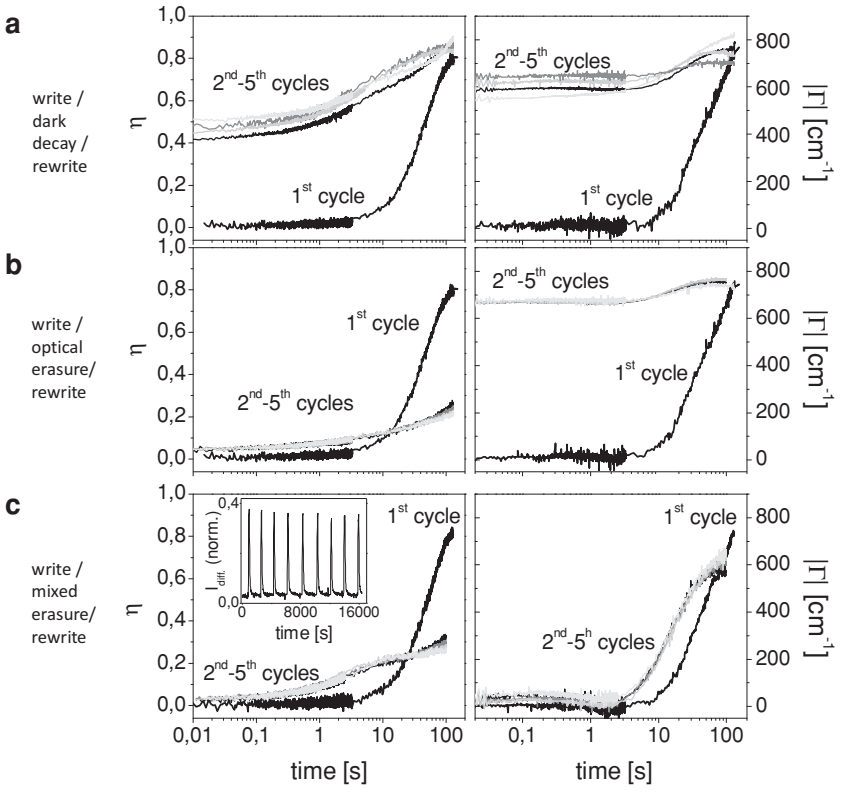

Figure 7. Different write/erase/write schemes for reversible holographic recording, in which, before rewriting, the sample was: a) kept for 30 min in the dark (both WBs were blocked), b) uniformly illuminated for 15 min (WB_2 was blocked), or c) first uniformly illuminated for 15 min and then kept in the dark for further 15 min. Grating buildup curves (η, left, and Γ, right) in the pristine sample (black lines) and after successive cycles (decreasing gray levels) are displayed (decay curves are not shown). Inset in (c): normalized RB diffracted intensity along 8 cycles 2 min-write/30 min-erase. Experiments were performed on a 35 µm **DR1-GP** sample using a recording transmission geometry ($\theta_1 = 26°$, $\theta_2 = 34°$).

which further provided relevant insights into the mechanisms governing the material behavior. We analyzed the evolution of a recorded grating under either dark conditions (dark decay) or uniform illumination (optical erasure), and posterior rewriting. Finally, we demonstrated efficient reversible holography using mixed erasure.

The first approach (**Figure 7**a), allowing grating relaxation for 30 min, was equivalent to the experiment shown in Figure 5 (both WBs were blocked) except for the length of time keeping the sample in the dark. Figure 7a shows that an important fraction of the grating was stable, even after long times (typically, 40–60% of the diffraction efficiency remained after 2 months, or even 70–80% if recording was performed for several hours). This proves the material potential for long-term storage applications, similarly to other photochromic materials previously reported.[2,3] By rewriting (in this and further cycles), the maximum η value was quickly recovered, showing a 15-fold faster buildup. Contrary to Figure 5, keeping the sample longer in the dark perturbed the behavior of Γ, which slightly decreased during dark decay and recovered by rewriting. In the second approach (Figure 7b), the sample was uniformly illuminated (in practice, by blocking one WB) to induce homogeneous alignment for 15 min. The grating was efficiently erased, as η almost completely vanished after few minutes, although Γ mostly remained unaltered. By rewriting, growth rates were moderately faster than in the first recording (ca. 5-fold) but η was strongly reduced. It must be noted that uniform illumination over longer times (above 20–25 min) led to reduced performance. Interestingly, both η and Γ curves were much more reproducible than after dark decay.

The grating behavior in these two experiments was consistent with the picture of PI-induced alignment occurring at two (molecular and domain) levels. Each erasure procedure affected in a different manner the grating modulation at only one or both levels (**Figure 8**). On the one hand, the stability of the grating during dark decay (small decrease of the modulation of Δn in Figure 8, top middle) indicated that spontaneous misalignment was inefficient in the dense high-T_g matrix, as discussed in the ellipsometric experiments (Figure 3b). Since such restrictions should affect more notoriously to microscopic structures, the domain stability will prevail. Thus, the moderate grating deterioration in the dark was mainly due to some randomization at the molecular level, while domains mostly retained their arrangement. The decay curves of both η and I_{ELP} (not shown) were biexponential, with fast and slow constant times of about 5 s and 200 s (attributable to molecular and domain relaxation, respectively). By rewriting, only the molecular alignment needed to be restored, which is much faster than reorganization motions at the microscale. Besides, the behavior of the optical gain shows that the grating shift mostly persisted, probably related to the domain stability. The relatively poor reproducibility of the cycles (Figure 7a) suggests that rewriting was quite sensitive to the exact grating progression during the dark periods. Note that the initial material centrosymmetry enables the high contrast of the first hologram as it allows Δn to remain close to 0 in the dark fringes (where the originally randomly oriented dye units are unaffected). This status does not change during this erase/write scheme, so the high hologram contrast is achieved again.

On the other hand, optical erasure succeeded (large decrease of the modulation of Δn in Figure 8, bottom middle) as the uniform irradiation led to homogeneous alignment of both molecules and domains, also including the former dark grating fringes (also confirmed by the increase of BR during erasure, measured by ellipsometry). The loss of modulation was almost complete although the persistence of the optical gain Γ (being calculated using the initial, i.e., before the first recording, beam intensities) demonstrated that the residual grating remained shifted. Note that the induced uniform alignment leads to an increase (on average) of Δn, but a reduced contrast (this fact, however, is unnoticed by η in the following write cycles, Figure 7b, left, since the diffraction efficiency only depends on the spatial

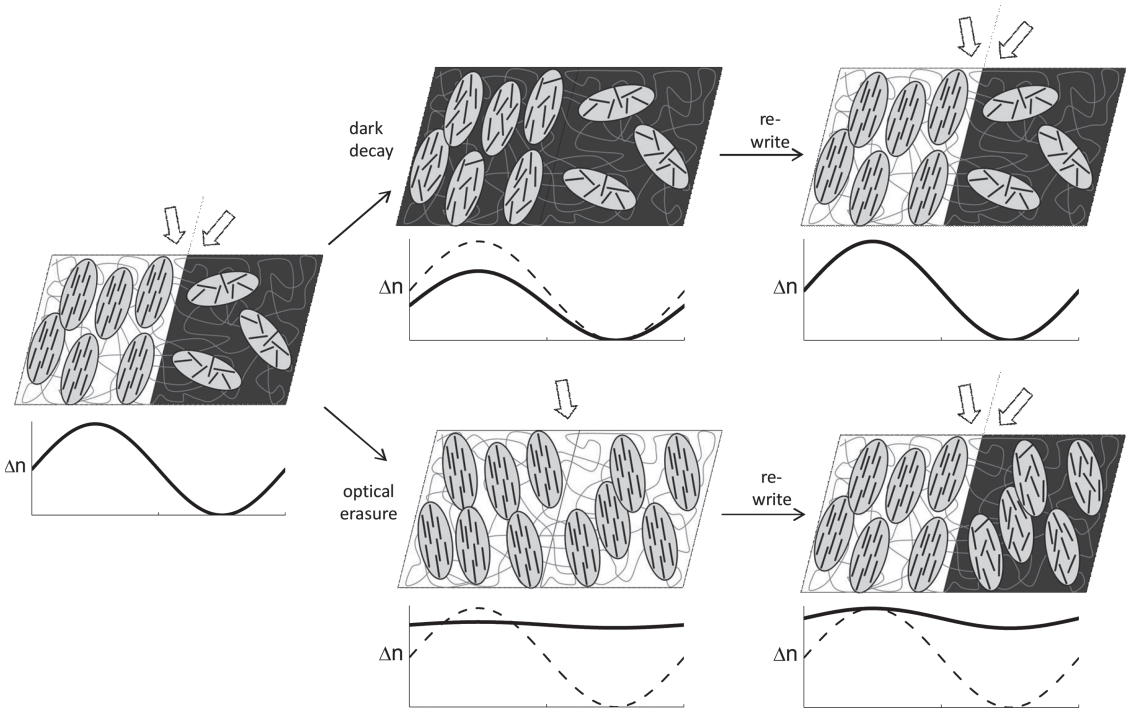

Figure 8. Sketch of the grating evolution along reversible recording schemes, in which the sample is either kept in the dark or uniformly illuminated before rewriting. White and black areas represent bright and dark pattern fringes, respectively. Photoisomerizable (DR1-containing) units (small black rods) are able to re-orient in the bright fringes upon illumination, also promoting the alignment of microscopic domains (gray ellipsoids). On the contrary, the randomly oriented chromophore units, given the initial material centrosymmetry, are not affected in the dark fringes. Relaxation processes in the dark, predominantly at the domain level, are restricted by the rigid silica network (denoted by the curled line at the background) and the dense chromophore content. The PI-induced spatial (sinusoidal) modulation of the refractive index (Δn) is represented in each case (dashed line is the original Δn modulation, i.e., after the first writing).

modulation of Δn along the grating). Again, the decay of η during erasing was biexponential, with constant times scaling of the intensity of the erasure beam. Even though the grating was erased, rewriting was faster than the first writing, suggesting a memory effect in the material,[38] probably allowed by the deformed silica network and favored by the already formed microdomains. Note that the speed improvement was less pronounced than after dark decay, likely because domain realignment is involved in this case. However, dark fringes retained after rewriting most of the alignment, which strongly reduced the maximum grating contrast achievable.[39] This explains the loss of performance, not profiting from the high hologram contrast allowed by the initial material centrosymmetry, similarly to the case of pre-poled samples discussed above; note that sample poling or pre-illumination did not improve the response time, contrary to the behavior found here, as no memory effects were involved. The worsened performance obtained by erasing over longer times suggests that nearly irreversible homogeneous alignment can be induced.

Both recording schemes were unsatisfactory for rewritable holography, since the first approach did not effectively erase the hologram, while the second approach led to strong loss of grating contrast and rather low increase of the buildup speed. A trade-off can be reached by combining both schemes: the sample was uniformly illuminated for 15 min and kept in the dark for further 15 min (Figure 7c). The hologram was almost completely erased but showing an acceptable diffraction efficiency by rewriting (30–40% of the original grating) and about 20-fold increased buildup rate. Γ almost vanished as well, and it practically recovered the original value. Such improvement must be attributed to the misalignment of the dye molecules in the dark fringes allowed during no illumination, after grating erasure. The Γ disappearance suggests that no residual phase-shift remained after the combined erasure. The loss of grating contrast by rewriting is due to some persistent arrangement in the dark fringes. Note that the inverse procedure (dark decay followed by uniform illumination) was much less efficient as the homogeneous alignment induced at the second step prevailed. Both η and Γ curves in Figure 7c showed high reproducibility upon repeated optical erasure/rewrite cycles, which supports the suitability of the films for reversible recording, including photoswitching applications (inset).

To conclude, only erasure upon thermal treatment above T_g resulted in absolute randomization at both levels. Indeed, by heating the film at 130 °C for 10 min, the hologram was completely erased (not only η and Γ, but also the photoinduced BR vanished) and rewritten gratings exhibited identical performance as in the fresh sample. That is, the material history was lost (no memory was preserved) and the material recovered its pristine state. The fatigue-resistance to the thermal erasure was remarkable and the holographic performance barely degraded even after more than 50 heating cycles.

5. Conclusions

In summary, we have characterized in-depth a highly photoisomerizable sol–gel material consisting of a silica matrix heavily doped with the azo-chromophore DR1 (52 wt%). The material properties were analyzed by a broad number of experiments with emphasis on the holographic performance. In order to improve the dye photoresponse, the flexibility and internal free volume of the silica network was decisively increased by incorporating glycidoxypropyl groups. The lowered matrix T_g further allowed straightforward fabrication of thick optical films, in which chromophore aggregation was ruptured by simple thermal annealing without additional photochemical treatment. The matrix rearranged in an evaporation-induced process, leading to favorable dye structures but keeping material centrosymmetry (which enabled high hologram contrast). We proved the occurrence of cooperative motions promoted by the molecular photoalignment. The formation of microscopic domains, not previously demonstrated in sol–gel materials, positively contributed to the large PI material response (birefringence of 0.11 at low irradiation intensities). The photoalignment at both molecular and microscopic level directly affected the holographic recording. In particular, spatially shifted domains appeared to play a relevant role in the achievement of optical gain, so collective motions might be related to the non-local nature of the photoisomerization gratings. Different recording (write–erase–write) schemes procedures were investigated, proving the material suitability for either long-term or reversible holography.

This work provides a solid knowledge on the properties and acting mechanisms in this novel material, and identifies some key aspects for further performance enhancement, especially regarding the dynamic range. On the one hand, a more flexible silica backbone or chromophore attachment by noncovalent bonds should be explored for improved material response without compromising stability and chromophore load. On the other hand, optimized recording configurations (for example, using reflection geometry and combined erase/re-write procedure) will accelerate the grating speed as well, which is of interest for specific applications.

6. Experimental Section

Material and Film Preparation: Acid hydrolysis (8 mmol of H_2O, pH = 1) of sol–gel precursors was accomplished at 65 °C in pyridine solvent (2.5 mL). The conditions of gelation prevented the polymerization of the GP groups,[40] as verified by FTIR spectroscopy. The sol was filtered (0.45 μm) to remove particle impurities. After filtering, the reaction was allowed to proceed until the sol reaches a maximum viscosity, which was then casted on an indium tin oxide (ITO) glass. Micrometer-thick sandwich-like films were obtained by placing a glass slide on top of the sample prior to its gelation at room temperature. The sample thickness (d) was controlled by glass spacers. For sample annealing, the upper glass slide was removed after 24 h and the film was readily tempered on a hot plate at 150 °C for 10 min. After shrinkage of 4–8% due to the annealing, d ranged between 2 and 102 μm. When the application of an external electric field was needed, a second ITO glass was glued on top of the annealed sample. Pre-poled samples were prepared by corona poling (a voltage of 5.6 kV was applied by a tungsten needle electrode held at 1 cm above the film), performed simultaneously to thermal annealing.

By contrast to other hybrid optical materials, this procedure allowed easy fabrication of reproducible, plane-parallel films with large areas (up to 4 cm^2) and controllable thickness above 100 μm. After annealing, bubble-free, non-scattering, and transparent films were attained, exhibiting excellent optical quality for more than three years after preparation, with no sign of chromophore aggregation or phase segregation under regular laboratory conditions. Both annealed and non-annealed films were rigid and very stable against mechanical strain.

Glass transition temperatures (T_g) and chromophore load were measured by means of both differential scanning calorimetry (DSC) and thermogravimetry with a Mettler Toledo DSC/TGA 1 apparatus, during the second heating cycle (rate of 20 K min^{-1}). Absorbances (A) were measured with a Cary Variant UV-Vis spectrophotometer in films of d = 2 μm. Absorbance changes were measured in situ by coupling 633 nm light into the spectrometer. Absorption coefficients α were calculated as $\alpha = \ln 10\ A/d$ before irradiation. Films were inspected by atomic force microscopy (Veeco), field emission SEM (FEI Nova NANOSEM 230), and polarized optical microscopy (Nanofilm). Mechanical stiffness was measured on 12 μm thick samples with a NanoTest platform (Micromaterials Ltd.)

Ellipsometry and Electro-Optical Measurements: Null-transmission ellipsometric[41] measurements were performed using a weak NIR probe beam (λ_{ELP} = 785 nm), which illuminates the sample placed between two crossed polarizers, set at ±45° with respect to the plane of incidence (Figure 3a, inset). The internal angle of incidence θ was 29°. Assuming that the probe beam does not induce PI, light transmission is due to both photoinduced birefringence and EO effect, according to (for symmetry C_∞):[42]

$$I_{ELP} = \sin^2\left(\frac{2\pi d}{\lambda_{ELP}\, G}\left(|n_e - n_o| + \frac{n^3(r_{33} - r_{13})E}{2}\right)\right) \quad (1)$$

where I_{ELP} is the (normalized) transmitted intensity of the probe beam, $|n_e - n_o|$ is the birefringence (BR), where n_e and n_o are the refractive indices referred to the extraordinary – parallel to the sample plane – and ordinary – perpendicular to the sample plane – axes, respectively, r_{33} and r_{13} the EO coefficients, and $G = n(n^2 - \sin^2\theta)^{1/2}/\sin^2\theta$ is a geometric factor (n is the average material refractive index, about 1.7, yielding G = 11.8). Measurements of r_{33} and r_{13} were carried out by using a Mach-Zehnder interferometric setup.[43] Hereby, the origin of axis 3 (normal to the sample) is set on the film/glass surface.

Holographic Experiments: Photoisomerization gratings were induced by the light-intensity modulated interference pattern resulting from the overlap of two coherent 633 nm WBs within the sample, without applying electric field. A HeNe laser (30 mW output) was used to generate p-polarized WB_1 and WB_2 with incident angles θ_1 and θ_2, both having equal internal intensities (200 mW cm^{-2}). The subindex 1 designates the beam closer to the sample normal (see inset in Figure 5). Diffraction properties of the recorded hologram were characterized by degenerate four-wave-mixing (DFWM). Thereby, a weak independent p-polarized read beam (RB) of the same wavelength with incident intensity $I_{RB,inc}$, and counter-propagating to one WB is diffracted by the recorded grating into the direction of the other WB (see inset in Figure 5). The internal diffraction efficiency η is directly calculated from DFWM measurements according to

$$\eta = \frac{I_{RB,diff}}{I_{RB,trans} + I_{RB,diff}} \quad (2)$$

where $I_{RB,trans}$ and $I_{RB,diff}$ are, respectively, the transmitted and diffracted RB intensities after the sample. Assuming thick transmission holograms,[44] the index modulation of the grating, Δn, can be obtained from η according to

$$\eta = \sin^2\left(\frac{\pi d \Delta n}{\lambda (\cos\theta_1 \cos\theta_2)^{1/2}}\right) \quad (3)$$

where λ is the RB wavelength and $\theta_{1,2}$ are the incidence angles of $WB_{1,2}$. In thick reflection gratings, Δn can be obtained from the external diffraction efficiency ($\eta_{ext} = I_{RB,diff}/ I_{RB, inc}$) according to[44,45]

$$\eta_{ext} = 1/\left(\xi/\nu + \sqrt{1 + \xi^2/\nu^2}\coth\sqrt{\nu^2 + \xi^2}\right)^2 \quad (4)$$

$$\nu = \frac{\pi d\,|\Delta n_p|}{\lambda\sqrt{-\cos\theta_1\,\cos\theta_2}}\,|\cos(\theta_2 - \theta_1)| \quad (5)$$

with $\xi = \alpha d\,(1/\cos\theta_1 - 1/\cos\theta_2)/4$, which includes the absorption coefficient α. Note that ν is a real-valued parameter since $(\cos\theta_1\cos\theta_2) < 0$ in reflection gratings.

Two-beam coupling (TBC), common in PR studies but very rare in photoisomerization studies, was used to investigate the energy exchange between WBs (optical gain). Thereby, the internal intensities of $WB_{1,2}$ were measured before ($I_{1,2}(0)$) and after/during ($I_{1,2}$) recording, and the gain coefficient Γ obtained as

$$\Gamma = \frac{1}{d}\left(\ln\frac{I_1(0)}{I_1} - \left|\frac{\cos\theta_2}{\cos\theta_1}\right|\ln\frac{I_2(0)}{I_2}\right) \quad (6)$$

Non-vanishing Γ is a signature of non-local gratings, i.e. the index grating is phase-shifted with respect to the light-interference pattern. A positive (negative) Γ implicates that WB_1 gains (loses) energy.

In dynamic measurements, buildup rates were estimated in each case by the half-time τ_{50}, given by the time needed to reach half the steady-state value. The stability of both the recording laser and the optical setup was verified during all holographic measurements by an auxiliary Mach-Zehnder interferometer, which allows ruling out of spurious contributions to the optical gain. Absorption losses and reflection at the interfaces were considered in all calculations. No light guiding was observed in the film.

Acknowledgements

The authors thank Alexander Ruhl (University of Cologne) for polarized optical microscopy measurements. This work was supported by the European Space Agency (ESA, MAP AO 99-121) and the Germany Ministry of Science and Education (BMBF, project 50WB0730). F.d.M. thanks MAT2009-10214 for financial support.

Received: May 11, 2012
Revised: January 17, 2013
Published online: February 27, 2013

[1] P. Günter, *Nonlinear Optical Effects and Materials*, Springer Verlag, Berlin **2000**.
[2] J. A. Delaire, K. Nakatani, *Chem. Rev.* **2000**, *100*, 1817.
[3] A. Natansohn, P. Rochon, *Chem. Rev.* **2002**, *102*, 4139.
[4] a) C. J. Barrett, A. L. Natansohn, P. J. Rochon, *Phys. Chem.* **1996**, *100*, 8836; b) M. Han, T. Honda, D. Ishikawa, E. Ito, M. Harab, Y. Norikane, *J. Mater. Chem.* **2011**, *21*, 4696.
[5] F. Gallego-Gómez, A. Blanco, D. Golmayo, C. López, *Adv. Funct. Mater.* **2011**, *21*, 4109.
[6] a) T. Todorov, L. Nikolova, N. Tomova, *Appl. Opt.* **1984**, *23*, 4309; b) W. M. Gibbons, P. J. Shanmon, S.-T. Sun, B. J. Swettlin, *Nature* **1991**, *351*, 49; c) S. Hvilsted, C. Sánchez, R. Alcalá, *J. Mater. Chem.* **2009**, *19*, 6641.
[7] a) R. H. Berg, S. Hvilsted, P. S. Ramanujam, *Nature* **1996**, *383*, 505; b) P. H. Rasmussen, P. S. Ramanujam, R. H. Berg, S. Hvilsted, *J. Am. Chem. Soc.* **1999**, *121*, 4738.
[8] a) S. J. Zilker, T. Bieringer, D. Haarer, R. S. Stein, J. W. van Egmond, S. G. Kostromine, *Adv. Mater.* **1998**, *10*, 855; b) V. Cimrová, D. Neher, S. Kostromine, Th. Bieringer, *Macromolecules* **1999**, *32*, 8496.
[9] O. Ostroverkhova, W. E. Moerner, *Chem. Rev.* **2004**, *104*, 3267.
[10] S. Köber, M. Salvador, K. Meerholz, *Adv. Mater.* **2011**, *23*, 4725.
[11] a) E. Mecher, F. Gallego-Gómez, H. Tillmann, H. H. Hörhold, J. C. Hummelen, K. Meerholz, *Nature* **2002**, *418*, 959; b) K. Roy Choudhury, Y. Sahoo, P. N. Prasad, *Adv. Mater.* **2005**, *17*, 2877; c) H. Li, R. Termine, L. Angiolini, L. Giorgini, F. Mauriello, A. Golemme, *Chem. Mater.* **2009**, *21*, 2403; d) F. Gallego-Gómez, J. A. Quintana, J. M. Villalvilla, M. A. Díaz-García, L. Martín-Gomis, F. Fernández-Lázaro, A. Sastre-Santos, *Chem. Mater.* **2009**, *21*, 2714; e) P.-A. Blanche, A. Bablumian, R. Voorakaranam, C. Christenson, W. Lin, T. Gu, D. Flores, P. Wang, W.-Y. Hsieh, M. Kathaperumal, B. Rachwal, O. Siddiqui, J. Thomas, R. A. Norwood, M. Yamamoto, N. Peyghambarian, *Nature* **2010**, *468*, 80.
[12] F. Gallego-Gómez, F. del Monte, K. Meerholz, *Nat. Mater.* **2008**, *7*, 490.
[13] C. Sanchez, B. Lebeau, F. Chaput, J.-P. Boilot, *Adv. Mater.* **2003**, *15*, 1969.
[14] Themed issue on *Recent Progress in Hybrid Materials Science*, guest eds. C. Sanchez, K. J. Shea, S. Kitagawa, *Chem. Soc. Rev.* **2011**, *40*.
[15] a) F. Chaput, D. Riehl, J. P. Boilot, K. Cargnelli, M. Canva, Y. Lévy, A. Brun, *Chem. Mater.* **1996**, *8*, 312; b) B. Lebeau, C. Sanchez, S. Brasselet, J. Zyss, G. Froc, M. Dumont, *New J. Chem.* **1996**, *20*, 13; c) B. Darracq, M. Canva, F. Chaput, J. P. Boilot, D. Riehl, Y. Lévy, A. Brun, *Appl. Phys. Lett.* **1997**, *70*, 292.
[16] Z. Sekkat, W. Knoll, *Photoreactive Organic Thin Films*, Academic Press, New York **2002**.
[17] R. Loucif-Saibi, K. Nakatani, J. A. Delaire, *Chem. Mater.* **1993**, *5*, 229.
[18] a) T. M. Long, T. M. Swager, *J. Am. Chem. Soc.* **2002**, *124*, 3826; b) E. Ishow, R. Camacho-Aguilera, J. Guérin, A. Brosseau, K. Nakatani, *Adv. Funct. Mater.* **2009**, *19*, 796.
[19] F. Lagugné Labarthet, S. Freiberg, C. Pellerin, M. Pézolet, A. Natansohn, P. Rochon, *Macromolecules* **2000**, *33*, 6815.
[20] J. Reyes-Esqueda, B. Darracq, J. García-Macedo, M. Canva, M. Blanchard-Desce, F. Chaput, K. Lahlil, J. P. Boicot, A. Brun, Y. Lévy, *Opt. Commun.* **2001**, *198*, 207.
[21] P. Cheben, F. del Monte, J. D. Worsfold, D. J. Carlsson, J. D. Mackenzie, *Nature* **2000**, *408*, 64.
[22] C. T. Kresge, M. E. Leonowicz, W. J. Roth, J. C. Vartuli, J. S. Beck, *Nature* **1992**, *359*, 710.
[23] A PI response needed illumination at wavelengths being absorbed by the azo-chromophore. Photoirradiation at 633 nm ensured high absorption by our material (α = 450 cm^{-1}, see ref. [12]) but still allowed enough transmission along the sample. No optical response was observed using NIR wavelengths at either 780 or 830 nm.
[24] K. Ichimura, *Chem. Rev.* **2000**, *100*, 1847.
[25] O. V. Yaroshchuk, T. Sergan, J. Lindau, S. N. Lee, J. Kelly, L.-C. Chien, *J. Chem. Phys.* **2001**, *114*, 5330.
[26] I. Zebger, M. Rutloh, U. Hoffmann, J. Stumpe, H. W. Siesler, S. Hvilsted, *Macromolecules* **2003**, *36*, 9373.
[27] a) G. Cerveau, R. J. P. Corriu, E. Framery, F. Lerouge, *Chem. Mater.* **2004**, *16*, 3794; b) P. R. Giunta, R. P. Washington, T. D. Campbell, O. Steinbock, A. E. Stiegman, *Angew. Chem., Int. Ed.* **2004**, *43*, 1505.
[28] a) Y. Lu, H. Fan, N. Doke, D. A. Loy, R. A. Assink, D. A. LaVan, C. J. Brinker, *J. Am. Chem. Soc.* **2000**, *122*, 5258; b) S. H. Kim, M. J. Misner, T. Xu, M. Kimura, T. P. Russell, *Adv. Mater.* **2004**, *16*,

226; c) D. Grosso, F. Cagnol, G. J. de A. A. Soler-Illia, E. L. Crepaldi, H. Amenitsch, A. Brunet-Bruneau, A. Bourgeois, C. Sanchez, *Adv. Funct. Mater.* **2004**, *14*, 309.

[29] D. Riehl, F. Chaput, Y. Levy, J.-P. Boilot, F. Kajzar, P.-A. Chollet, *Chem. Phys. Lett.* **1995**, *245*, 36.

[30] B. Kippelen, N. Peyghambarian, *Adv. Polym. Sci.* **2003**, *161*, 87.

[31] Contrary to thicker samples, 2–4 µm thick samples exhibited lamellar-like anisotropic domains along the film plane, probably due to the silica structures being longer than the sample thickness. Nevertheless, their optical behavior was analogous.

[32] a) T. Seki, *Bull. Chem. Soc. Jpn.* **2007**, *80*, 2084; b) Y. Zhao, J. He, *Soft Matter* **2009**, *5*, 2686.

[33] a) A. Stracke, J. H. Wendorff, D. Goldmann, D. Janietz, *Liq. Cryst.* **2000**, *27*, 1049; b) K. Kreger, P. Wolfer, H. Audorff, L. Kador, N. Stingelin-Stutzmann, P. Smith, H.-W. Schmidt, *J. Am. Chem. Soc.* **2010**, *132*, 509.

[34] a) A. Natansohn, P. Rochon, M. Pezolet, P. Audet, D. Brown, S. To, *Macromolecules* **1994**, *27*, 2580; b) R. Hagen, T. Bieringer, *Adv. Mater.* **2001**, *13*, 1805; c) B. L. Lachut, S. A. Maier, H. A. Atwater, M. J. A. de Dood, A. Polman, R. Hagen, S. Kostromine, *Adv. Mater.* **2004**, *16*, 1746; d) K. Okano, O. Tsutsumi, A. Shishido, T. Ikeda, *J. Am. Chem. Soc.* **2006**, *128*, 15368.

[35] a) J. P. Chen, F. Lagugné-Labarthet, A. Natansohn, P. Rochon, *Macromolecules* **1999**, *32*, 8572; b) G. Iftime, F. Lagugné-Labarthet, A. Natansohn, P. Rochon, K. Murti, *Chem. Mater.* **2002**, *14*, 168.

[36] E. Mecher, F. Gallego-Gómez, K. Meerholz, H. Tillmann, H. Hörhold, J. C. Hummelen, *ChemPhysChem* **2004**, *5*, 277.

[37] These considerations also agree with the better defined structural organization observed in 2 µm films (Figure 3a). However, holographic performance in those samples is not comparable because the fringe spacing surpasses the film thickness (Raman-Nath regime[1]).

[38] a) J. Stumpe, Th. Geue, Th. Fischer, H. Menzel, *Thin Solid Films* **1996**, *284–285*, 606; b) M. Han, M. Kidowaki, K. Ichimura, P. S. Ramanujam, S. Hvilsted, *Macromolecules* **2001**, *34*, 4256; c) C. Sánchez, R. Alcalá, S. Hvilsted, P. S. Ramanujam, *Appl. Phys. Lett.* **2001**, *78*, 3944.

[39] The material behavior upon this approach is closely related to that observed using what we called gain steering technique by recording with assistance of a third independent beam (ref. [12]), in which the buildup was accelerated by sacrificing grating contrast.

[40] Y. Sorek, M. Zevin, R. Reisfeld, T. Hurvits, S. Ruschin, *Chem. Mater.* **1997**, *9*, 670.

[41] a) C. C. Teng, H. T. Man, *Appl. Phys. Lett.* **1990**, *56*, 1734; b) J. S. Schildkraut, *Appl. Opt.* **1990**, *19*, 2839.

[42] Sandalphon, B. Kippelen, K. Meerholz, N. Peyghambarian, *Appl. Opt.* **1996**, *35*, 2346.

[43] M. G. Kuzyk, C. W. Dirk, *Characterizations Techniques and Tabulations for Organic Nonlinear Optical Materials*, Marcel Dekker Inc., New York **1998**.

[44] H. Kogelnik, *Bell Syst. Tech. J.* **1969**, *48*, 2909.

[45] F. Gallego-Gómez, M. Salvador, S. Köber, K. Meerholz, *Appl. Phys. Lett.* **2007**, *90*, 251113.